Ceramics International 45 (2019) 22998–23006

Contents lists available at ScienceDirect

Ceramics International

journal homepage: www.elsevier.com/locate/ceramint

Insights into formation of anatase TiO_2 nanoparticles from peroxo titanium complex degradation under microwave-assisted hydrothermal treatment

Vagner R. de Mendonça[a,*], Osmando F. Lopes[b], Waldir Avansi Jr.[c], Raul Arenal[d,e], Caue Ribeiro[f,g]

[a] Federal Institute of Education, Science and Technology of São Paulo, IFSP Campus Itapetininga, 18202-000, Itapetininga, SP, Brazil
[b] Institute of Chemistry, Federal University of Uberlândia, Santa Mônica, 38400-902, Uberlândia, MG, Brazil
[c] Laboratory of Nanostructured Multifunctional Materials, Department of Physics - Federal University of São Carlos, P.O. Box 676, 13565-905, São Carlos, SP, Brazil
[d] Laboratorio de Microscopias Avanzadas, Instituto de Nanociencia de Aragon (INA) - Universidad de Zaragoza, Calle Mariano Esquillor, 50018, Zaragoza, Spain
[e] ARAID Foundation, 50018, Zaragoza, Spain
[f] Embrapa Instrumentation, Rua XV de Novembro, 1452, 13560-970, São Carlos, SP, Brazil
[g] Forschungszentrum Jülich GmbH, Institute of Energy and Climate Research (IEK-3): Electrochemical Process Engineering, 52425, Jülich, Germany

ARTICLE INFO

Keywords:
Phase evolution
Peroxo titanium complex
TiO_2 nanocrystal
Titanate
Microwave-assisted hydrothermal

ABSTRACT

Several methods for the synthesis of anatase TiO_2 have been reported in the literature. In particular, the microwave-assisted hydrothermal crystallization of Ti-peroxocomplexes has enabled the phase and morphological control of TiO_2 nanoparticles by adjusting the synthesis conditions, such as pH, time and temperature, with significant increase in the reaction rate compared to the conventional sol-gel techniques. In this paper, we uncover the mechanism involved in the formation of anatase TiO_2 nanoparticles from the Ti-peroxo complex precursor route. Structural characterizations (XRD, Raman, TEM and XANES) revealed that the Ti-peroxo complex precursor exhibits a titanate-like structure, comprised of bulk NH_4^+ ions and surface peroxo groups. The NH_4^+ ions release during hydrothermal treatment is determining on the anatase TiO_2 nanoparticle formation, which occurs concomitantly with the decomposition of peroxogroups. UV-induced dye photodegradation tests involving the Ti-peroxo complex precursor and TiO_2 nanoparticles showed that the precursor is not able to form hydroxyl radicals that are the main chemical species responsible for the dye photodegradation, despite the presence of peroxo groups at its surface. The results herein highlight the mechanism involved in the formation of anatase TiO_2 nanoparticles, which could assist in the development of new synthesis approaches based on Ti-peroxocomplex precursors.

1. Introduction

Nanoparticle growth mechanisms have received much attention due to the importance of controlling the size and morphology of nanoparticles for specific applications [1]. Various synthesis approaches have been developed for the tailoring of advanced materials, amongst them, the oxidant peroxide method (OPM), which consists in the formation of a metal:hydrogen peroxide complex and its further degradation under controlled conditions [2]. OPM has been successfully applied for the synthesis of different materials, such as TiO_2 [3], V-doped TiO_2 [4], $BiVO_4$ [5,6], $PbTiO_3$ [7], $PbHfO_3$ [8], Nb_2O_5 [9,10], V_2O_5 [11], WO_3 [12], $Na_2V_6O_{16}.3H_2O$ [13] and $Bi_4Ti_3O_{12}$ [14]. Nanoparticles having different sizes, morphologies and surface features can also be prepared through OPM [15,16].

Current researches have focused on synthesis routes based on green chemistry principles to obtain the required TiO_2 phase and, from an environmental point of view, water-soluble complexes have proved to be very promising for the synthesis of titania [17]. Specifically for TiO_2, highly concentrated Ti(IV)/H_2O_2 aqueous solutions exhibit an intense yellow color, which is characteristic of Ti-peroxo complexes [18]. The H_2O_2 excess is necessary to stabilize the solution, but H_2O_2 tends to decompose, resulting in O_2 evolution. When most H_2O_2 is consumed, a yellow gel is formed spontaneously [19]. The OPM has been applied for the obtaining of TiO_2 in different phases, from rutile TiO_2 in acidic environment to titanate structures in mild basic conditions [20].

Although the Ti-peroxo complex is well-described in the literature [21], the TiO_2 formation mechanism as well as the phase control through this approach are still unclear [17]. Aspects related to the synthesis parameters are commonly controversial. For instance, TiO_2 crystallization is pH-sensitive, and since the Ti-peroxo complex

* Corresponding author.
E-mail address: vrm@ifsp.edu.br (V.R. de Mendonça).
URL: https://itp.ifsp.edu.br/index.php/docentes/210-vagner-romito-de-mendonca (V.R. de Mendonça).

https://doi.org/10.1016/j.ceramint.2019.07.345
Received 2 April 2019; Received in revised form 3 June 2019; Accepted 29 July 2019
Available online 01 August 2019

preparation requires the use of ammonium solution, especially when metallic Ti is used, the pH control over the crystallization step becomes a difficult issue. In this sense, the use of solid precursors (precipitated compounds) dispersed in a medium with neutral or constant pH is a suitable way to attain a controllable synthesis environment, as proposed by Ribeiro et al. [20].

Despite the OPM-based synthesis of TiO_2 has been studied [15,20,22], the crystal growth mechanism from the solid precursor has not been elucidated yet. In this paper, we used the microwave-assisted hydrothermal synthesis to study the precursor evolution towards anatase TiO_2. The microwave-assisted hydrothermal treatment was applied due to the easy control of time and temperature and the increased reaction rate [23], thus enabling a deep control on the intermediate reactions by quenching the synthesis at specific times. Therefore, the understanding on the crystallization of the peroxo titanium complex at molecular level makes possible the control of polymorphs and morphology in TiO_2 nanoparticles, which are important aspects for optimized performances and establishment of clear morphology-property correlations [24].

2. Experimental

2.1. Synthesis

Titanium peroxo complex was prepared according to a previous report [20]. In a typical synthesis procedure, 1.0 g of metallic Ti powder (99.7%, Aldrich) was added to 240 mL of H_2O_2 mixed (28%, Synth) with 80 mL of NH_4OH (34%, Synth). The suspension was kept in an ice-water bath until the complete Ti dissolution, resulting in a transparent yellow colored soluble peroxocomplex solution. To obtain the powder precursor, the solution was heated until boiling and then immersed in an ice-water cooling bath. The resulting precipitate was kept under magnetic stirring overnight to release the H_2O_2 and NH_3 excesses and further freeze-dried to obtain the peroxo ammonium titanate precursor powder, termed as PAT.

The crystallization process was carried out by preparing a PAT suspension in water at concentration of 2 g L^{-1} (natural pH = 8.0). The microwave-assisted hydrothermal synthesis was performed in a CEM Discover reactor. The PAT suspension was transferred to a 10 mL glass tube and sealed with a Teflon® cap. The synthesis in the microwave oven was performed with a microwave irradiation source consisting of a magnetron tube operating at 2.45 GHz. The microwave heating protocol was initiated by increasing the power to 90 W in order to heat the solution to 170 °C. After the heating ramp, the reaction temperature was kept constant and the reaction times were changed from 2 to 60 min. After the required time, the reaction was stopped by thermal quenching by a compressed air flow. The pressure and the temperature were controlled by a pressure sensor and an IR thermometer, respectively. During the hydrothermal treatment, the solutions were stirred by a magnetic stir bar to ensure high thermal and chemical homogeneity. In order to ensure reproducibility, the heating up and cooling down periods were kept identical for all samples. After the hydrothermal treatment, the precipitate was centrifuged, washed twice with ethanol and dried at 60 °C. The samples were identified according to the hydrothermal treatment time. The same process was employed for the treatment in benzyl alcohol, which was carried out in order to infer about the mechanism followed by the sample during crystallization.

2.2. Characterizations

Powder X-ray diffraction (XRD) patterns were measured (at room temperature) on an X'Pert Pro (PANalytical B.V.) powder diffractometer operating with Cu *Kα* radiation (45 kV, 40 mA) in the reflection mode. Additionally, XRD measurements were also performed at different temperatures using the heating system (TTK-450) in a Shimadzu diffractometer XRD – 6100. This system was used to heat the sample in order to study the influence of temperature on the crystal structure. In this way, the XRD patterns were obtained for PAT at ambient temperature and heated at 250 and 300 °C. Raman spectroscopy was performed with a FT-Raman Bruker RFS 100/s, using the 1063 nm line of YAG laser. Attenuated total reflectance-infrared (ATR-IR) spectra were recorded on a Bruker Alpha FT-IR spectrometer with diamond ATR optics. The thermal properties of the samples were studied by thermogravimetric (TG) analysis, which was performed in a TA Q500 thermal analyzer (TA Instruments, New Castle, DE, USA). Sample (10.0 ± 1.0 mg) was heated in air atmosphere flowing at 60 mL min^{-1} and the heating rate was 10 °C.min^{-1}. Differential scanning calorimetry (DSC) was performed with a Q Series DSC Q800 (TA Instruments). Samples were weighed (8.0 ± 1.0 mg) in aluminum pans, which were sealed and heated at a rate of 10 °C.min^{-1} until 350 °C. An empty aluminum pan was used as a reference. .

XANES (X-ray Absorption Near Edge Structure) spectra were measured at the titanium (Ti) *K*-edge using the D04B-XAFS1 beam line with Si (111) channel-cut monochromator at the Brazilian Synchrotron Light Laboratory (LNLS). In brief, the Ti *K*-edge XANES spectra were collected from samples deposited on polymeric membranes in transmission mode at room temperature. The spectra were measured from 40 eV below and 150 eV above the edge, with an energy step of 0.3 eV near the edge region, where the energy calibration of the monochromator was checked using a Ti metal foil as a reference. To study the XANES spectra of the samples, the TiO_2 (anatase) and potassium titanate obtained as previously described [25], were employed as reference compounds.

Morphological analyses were performed with a LEO 1530 Gemini scanning electron microscope (SEM) operating at 5 kV. Conventional TEM and high-resolution (HR-TEM) studies were conducted on an image aberration-corrected FEI Titan-Cube microscope running at 300 kV, equipped with a Cs corrector (CETCOR from CEOS GmbH). Samples were prepared by dropping particle suspensions on a copper grid which was further allowed to dry in air.

2.3. Photocatalysis tests

To evaluate the photocatalytic performance of the synthesized materials, 3.0 mg of sample were immersed in 20 mL of an aqueous Rhodamine B dye (RhB) solution (5.0 mgL^{-1}), which was further transferred to a photo-reactor equilibrated at 20 °C and illuminated by six UVC lamps (TUV Philips, 15 W each – total power: 90 W, maximum intensity at 254 nm). The RhB degradation was monitored by recording the UV–vis spectrum (Shimadzu-UV-1601 PC spectrophotometer, λ_{MAX} = 554 nm) at different times of UV exposure [26].

The hydroxyl radical formation rate was determined from the detection of 2-hydroxyterephthalic acid, a highly fluorescent product formed by the reaction between hydroxyl radicals and terephthalic acid formed during UV irradiation [27]. For this analysis, sample suspensions with concentration of 100 mgL^{-1} were prepared in an aqueous solution of terephthalic acid (4.7×10^{-4} $molL^{-1}$) ($C_8H_6O_4$ - Aldrich, 98% purity) and NaOH (2.4×10^{-3} $molL^{-1}$) (Isofar, 98% purity). Aliquot parts of the suspension were placed in a fluorimeter with controlled temperature and magnetic stirring (Jasco FP-8500 - Xenon short arc lamp from Ushio - Jasco parts center, Model UXL-159 - with 150 W) and constantly illuminated with the light source of the spectrophotometer set a wavelength of 315 nm. The spectra were collected every 60 s, and the hydroxyl radical formation rate was assessed by the change of the PL intensity at 425 nm emitted from the 2-hydroxyterephthalic acid excited by the same spectrophotometer light source (λ = 315 nm). The peak intensity attributed to 2-hydroxyterephthalic acid is proportional to the hydroxyl radical concentration. The plot of fluorescence intensity *vs* UVC irradiation time is a straight line whose slope, identified as k_{OH}, is directly proportional to the hydroxyl radical formation rate [28].

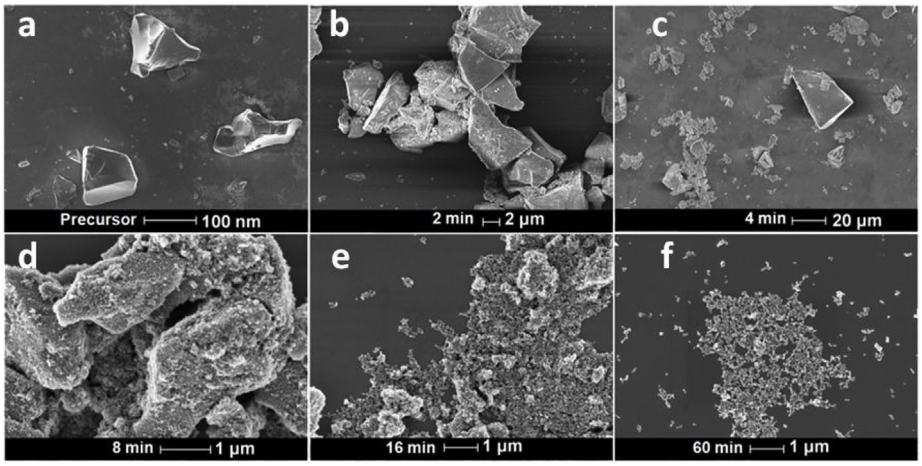

Fig. 1. Scanning Electron Mycroscopy images of representative samples: a) Precursor sample – PAT; samples hydrothermally treated at different times: b) 2 min; c) 4 min; d) 8 min; e) 16 min; f) 60 min.

3. Results and discussion

The peroxo ammonium titanate precursor powder (PAT) was first obtained by freeze-drying the gel formed from the dissolution of metallic Ti in H_2O_2/NH_4OH solution, as earlier described [20]. The freeze-drying technique was used to prevent the PAT from temperature-induced crystallization [15]. The PAT powder showed a yellow color attributed to the peroxo groups [29]. The reaction for the peroxo titanium complex formation occurs with the release of H_3O^+. Therefore, in order to improve the reaction yield, it is necessary to carry out the synthesis in an alkaline medium, which is achieved by the use of NH_4OH. The conversion of PAT to anatase TiO_2 in the microwave-assisted hydrothermal treatment leads to a white powder, indicating the full decomposition of the PAT peroxo groups.

Fig. 1 displays representative SEM images of the samples, in which the evolution of particle morphology with the hydrothermal treatment time is clearly visible. The SEM image of PAT presents micrometric particles which were shattered with the increasing treatment time. The surface roughness visible in the SEM image of the sample obtained after 8 min of hydrothermal treatment indicates a structural change in the solid. The sample treated for 60 min showed spherical nanoparticles diameter of around 20 nm without agglomeration.

Fig. 2 shows representative TEM images and their respective Fourier transform (FT) from selected regions of PAT and samples treated for 4, 8 and 16 min. It is clearly observed that PAT presents micrometric particles with low crystallinity, as verified by XRD (Fig. 3). The TEM images of the samples treated for 4 and 8 min show the presence of agglomerates containing some crystalline regions. It is worth mentioning that the amount of these crystalline regions is proportional to the hydrothermal treatment time. The FT data obtained from these regions suggest that these crystalline regions could be indexed to anatase TiO_2. Indeed, the TEM image of the sample treated for 16 min reveals the formation of crystalline TiO_2 nanoparticles with a poorly defined morphology.

XRD patterns (obtained at room temperature) are depicted in Fig. 3. Interestingly, the XRD pattern of PAT could be identified as titanate-like structures with a lamellar feature [30] by the broad peak at around 10°, which is typical of interlayer diffraction. The most intense peak of titanate-like phase remains even after 8 min of hydrothermal treatment, indicating a mixture of anatase TiO_2 and PAT. After 16 min, only anatase phase was identified by XRD. Therefore, even employing mild conditions (170 °C for 16 min) the method proposed here was efficient at producing anatase TiO_2 nanoparticles.

Fig. 4 shows the Raman spectra of the samples. In Fig. 4(a), the dotted lines indicate the Raman shifts related to the titanate-like structure [25], while the Raman shifts of anatase TiO_2 are indicated in Fig. 4(b) [31]. The PAT sample displayed Raman shifts similar to the titanate-like phase [25,32,33]. As a matter of fact, Fig. 4(c) presents the Raman spectra of PAT and potassium titanate obtained as per a previously described protocol [25]. In accordance with the XRD data, the peaks related to the titanate phase are identified in the spectra of the samples treated up to 8 min. As expected, longer hydrothermal treatment times lead to samples only comprised of anatase TiO_2, which is in good agreement with XRD.

ATR-IR analyses (Fig. 5) indicate the surface groups present in the PAT structure. The bands in the region 3000-3300 cm^{-1} could be ascribed to the N–H vibration modes. Additionally, the bands at 3300-3500 cm^{-1} are dominantly attributed to the OH groups bounded to the solid surface [34]. It is clear the displacement of these bands with the increasing hydrothermal treatment time, indicating a change in the Ti–OH bond force [35]. The bands at 1200 cm^{-1} were not identified in the spectra of the PAT samples, but were readily detected in the spectra of the sample treated for 2 min, which indicates a structural change after the hydrothermal treatment. The peak at 1630 cm^{-1} is attributed to the bending vibration of water molecules. The band observed at 900 cm^{-1} is assigned to $\upsilon_{O\text{-}O}$ and $\upsilon_{Ti\text{-}O2}$ modes of coordinated peroxide [36] and the strong band at 1395 cm^{-1} is related to the υ_4 mode of NH_4^+ associated with residual ammonium used in the preparation of PAT [37]. The bands at 900 and 1395 cm^{-1} disappeared after 16 min of hydrothermal treatment, which is consistent with the other results, meaning that only anatase TiO_2 phase is formed in these conditions. On the other hand, both results indicate that intermediate PAT fractions may be present in the samples treated up to 8 min, indicating that proper anatase formation only took place when the PAT structure was totally degraded.

In view of the structural similarity between PAT and titanate structures [24], and considering the existence of ammonium ions in the PAT composition, we propose that PAT has a titanate anion structure comprised of ammonium cations and peroxo groups at stoichiometric ratios. Additionally, the release of these ammonium cations during hydrothermal treatment and decomposition of peroxo groups are the main steps responsible for the anatase phase formation.

Fig. 6(a) presents the thermogravimetric (TG) and differencial thermogravimetric (DTG) profiles of PAT. Two thermal events at 130 °C and 240 °C, which can be related to water release and ammonium and peroxo groups decomposition, respectively, are consistent with previous data. After these thermal events, the sample weight remained almost constant at higher temperatures. Fig. 6 (b) shows the DSC curve of PAT. The exothermic peaks between 200 and 250 °C coincide with the highest weight loss rate in the TG/DTG curves and are possibly

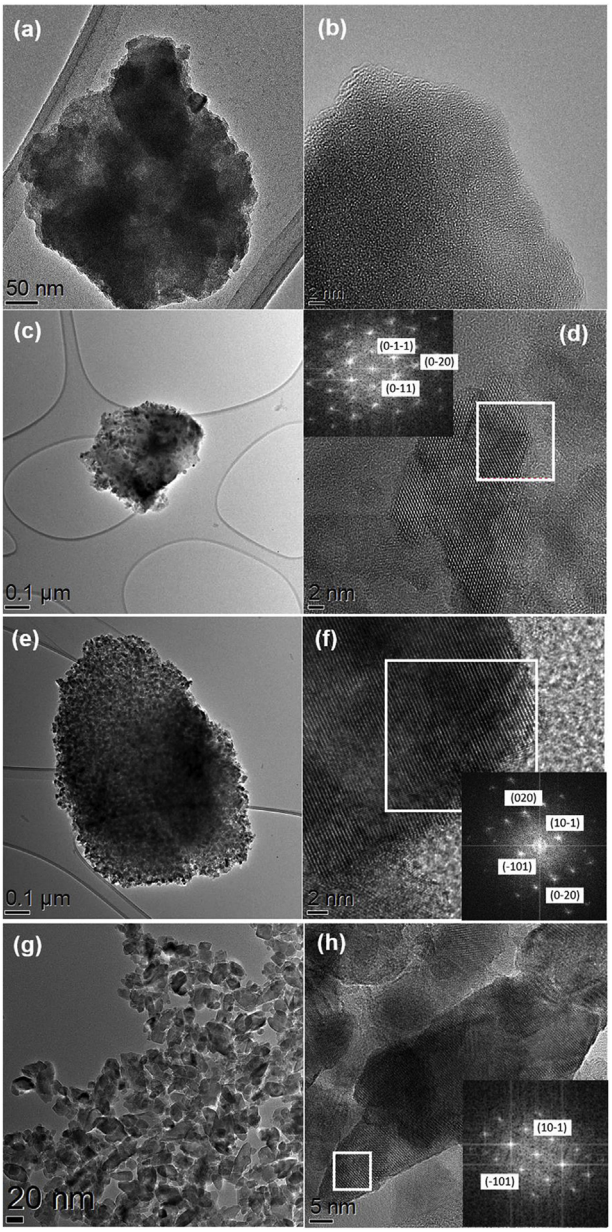

Fig. 2. High-resolution transmission electron microscopy images of representative samples: a) and b) Precursor sample - PAT; c) and d) 4 min; e) and f) 8 min; g) and h) 16 min. The respective Fourier Transform (FT) diffractograms are included as inserts, confirming the presence of anatase TiO_2.

ascribed to the peroxo groups decomposition [29], but it can also be relates to the oxidation of residual nitrogen. The event around 350 °C can be related to a crystallization step.

To gain a deep understanding and confirm the PAT structure, variations in the electronic and local atomic structure of the samples were studied. In this way, the PAT sample was examined by XANES and the resulting spectrum was compared with TiO_2 (anatase) and potassium titanate that were employed as reference compounds, Fig. 7(a). As a matter of fact, Fig. 7(b) presents the typical four major effects related to Ti compounds, which have already been reported [38,39]. The peaks A_3 and B are usually attributed to the 1s – 3d transitions and assigned to 1s- $2t_{2g}$ and 1s - $3e_g$ transitions in an octahedral field, respectively [38]. Although the origin of the A_1 (4968.7 eV) peak is considered by several works as less clear, it is also commonly attributed to the Ti 3d-4p hybridized state [38]. More importantly, the peak A_2 (4970.6 eV), attributed to five-coordinate titanium species due to a reduction in the average coordination number of titanium in samples with high surface area [39], is clearly observed for PAT and potassium titanate with intensity significantly higher than that for anatase TiO_2 samples. Ribeiro et al. observed a similar behavior for a peroxo titanium complex gel structure, in which the peroxocomplex was not related to the resulting rutile phase [40]. Mourão et al. also reported that the crystalline potassium titanate phase displays a similar behavior compared to anatase TiO_2 nanostructures [25], with a high intense peak related to five-coordinate titanium species [41]. Therefore, based on the XRD and Raman results, the XANES spectra also evidenced the similarity between the PAT and titanate structures concerning the Ti local order. It is interesting to note that when titanium isopropoxide was employed as a Ti source rather than the metallic Ti, the resulting material structure was similar to that presented here [25]. In this way, the titanate-like phase structure can be obtained even changing, at some extension, the chemicals used in the synthesis of TiO_2.

Thus, we propose that the anatase phase formation occurs with the release of ammonium ions and peroxogroups decomposition, as demonstrated in the adapted Scheme 1 [42]. The peroxo groups present at the samples surface can be used as a structure-direct agent during the synthesis, and its amount can be tuned by the pH [20,43]. During the microwave-assisted hydrothermal treatment, the ammonium ions diffuse through the solution and are further released as ammonia gas, since temperature governs the ratio between free ammonia and ammonium ions (NH_4^+) in an aqueous ammonia thermodynamic system [44]. Therefore, due to the ammonia gas evolution, the system becomes poor in positively charged ammonium ions, which are necessary to stabilize the negatively charged titanate layers, thereby resulting in anatase TiO_2 formation due to a rearrangement of the crystal structure [45]. Important to note that the formed polymorph in this step depends on the environmental pH, since strongly acid medium can results in rutile phase [20]. The same is valid to the morphology due to the fact

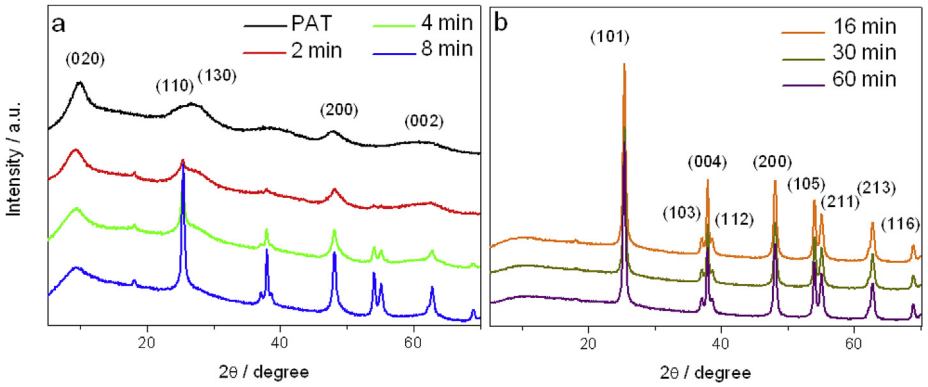

Fig. 3. XRD patterns of the as-synthesized samples: a) PAT; 2 min; 4 min; 8 min; b) 16 min; 30 min; 60 min. In (a) the indexes are related to the titanate phase (JCPDS 84–2057), while in (b) the indexes are related to the anatase TiO_2 phase (JCPDS 21–1272). The peak at around 18° is due to the sample holder.

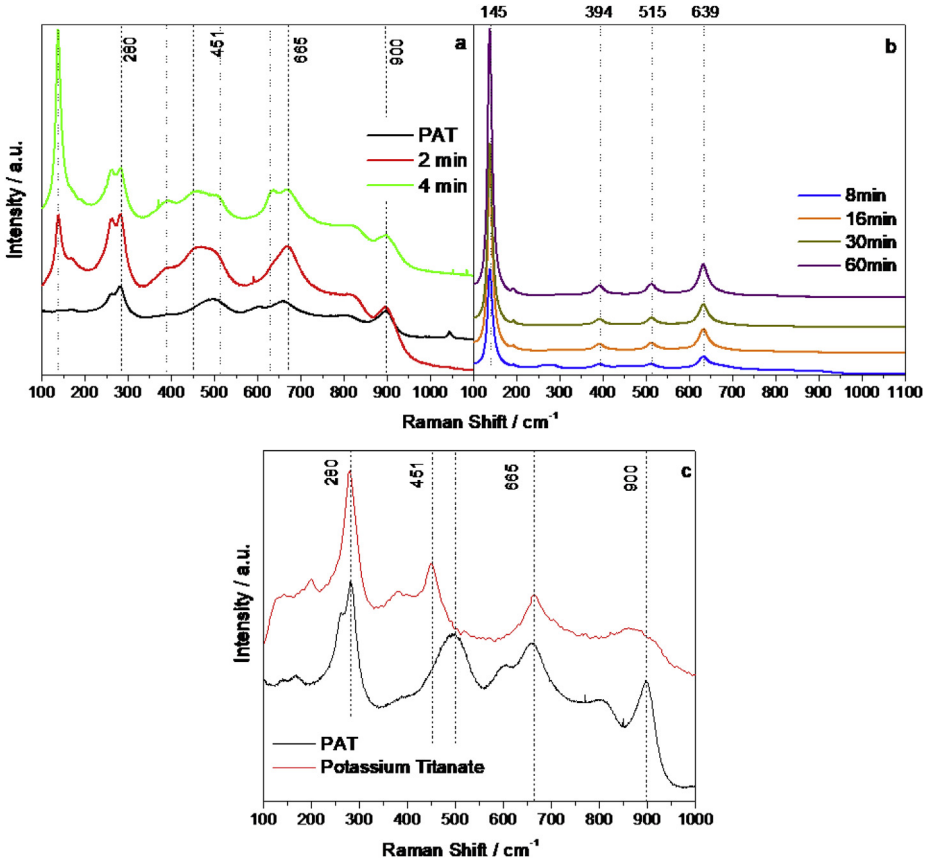

Fig. 4. Raman spectra of the PAT and samples treated at different times. (a) Raman shifts of titanate structures; (b) Raman shifts of anatase TiO_2; (c) Raman spectra of Potassium Titanate and PAT.

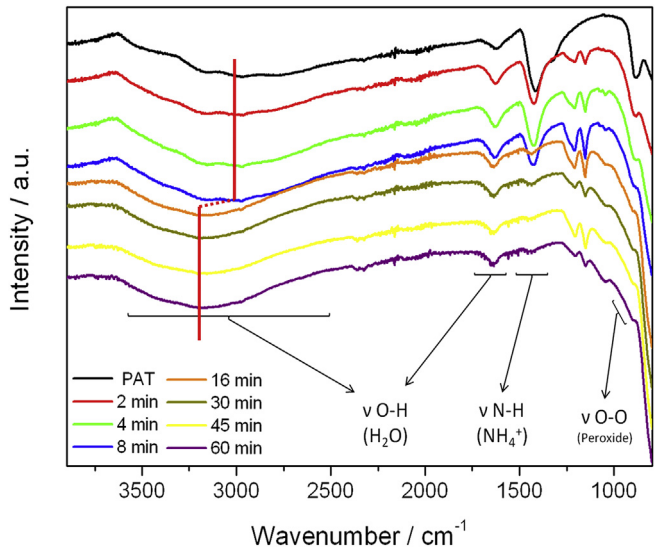

Fig. 5. ATR-IR spectra of PAT and samples treated for 2 min, 4 min, 8 min, 16 min, 30 min, 45 min, 60 min (from the top down).

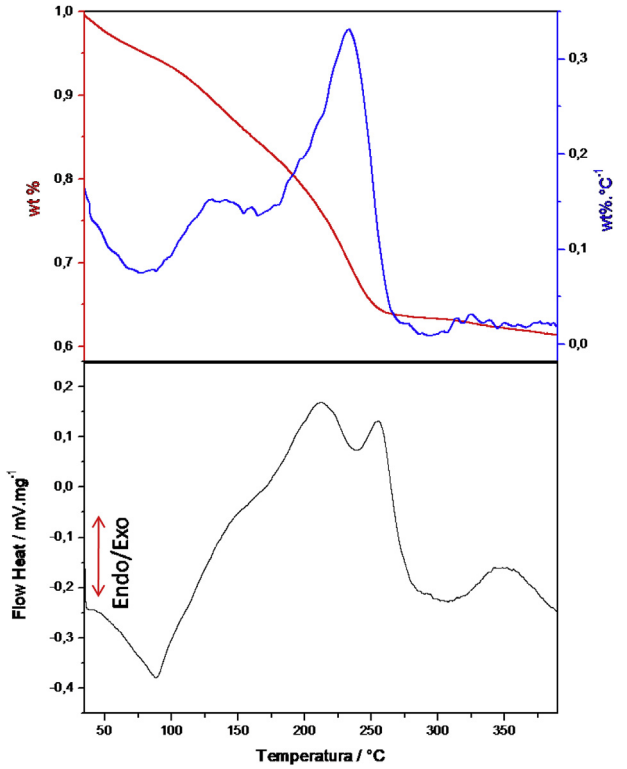

Fig. 6. Thermal analysis of PAT: a) Thermogravimetric (TG) profile in air atmosphere; b) DSC curve.

that slight variations of the pH can result in different morphologies of the same polymorph [15].

It has been previously shown that a highly alkaline medium is necessary to synthesize titanate structures [46]. However, Ribeiro et al. [20] proposed a method employing the PAT precursor by which it was possible to obtain titanate structures using base concentrations as low as 1 $molL^{-1}$. This occurs due to the ionic radius of the ammonium ions, which facilitates its release and exchange by K^+ ions. This method can

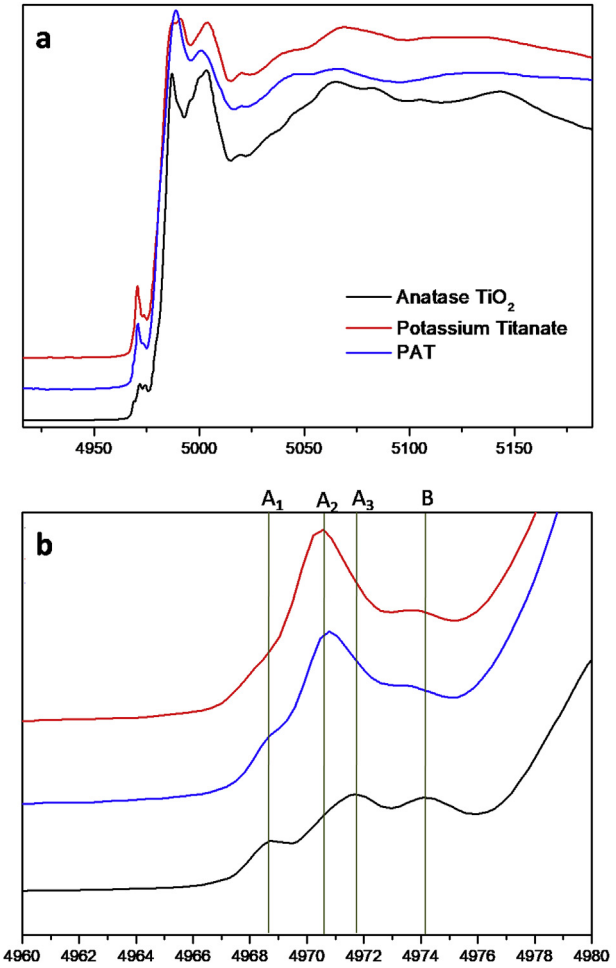

Fig. 7. a) Normalized Ti K-edge XANES spectra of PAT and reference compounds (anatase TiO_2 and Potassium Titanate); b) expanded view of pre-edge features of XANES spectra presented in (a).

be understood as the use of a precursor already exhibiting a titanate-like structure, further occurring only the cation exchange reaction depending on the base used in the synthesis. Other works have proposed a similar mechanism for the crystalline TiO_2 phase formation from titanates under different conditions, being the resulting phase related to hydrothermal treatment parameters or ionic species present in the

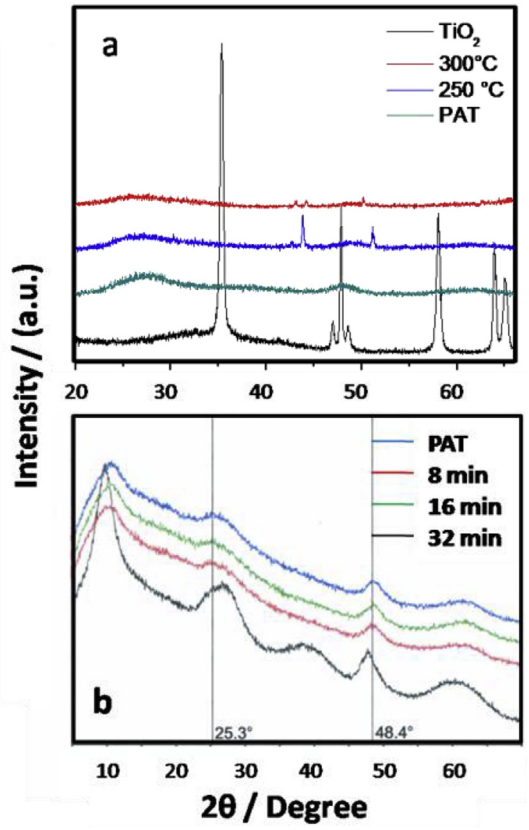

Fig. 8. XRD pattern of PAT treated: a) at different temperatures; b) treated at 170 °C in BnOH.

synthesis process [42,47].

To confirm this hypothesis, we performed two different experiments. Initially, we performed XRD measurements on samples treated at different annealing temperatures based on the thermal analysis results. Fig. 8 (a) presents the XRD patterns of the anatase TiO_2 (reference sample – Titanium (IV) oxide, anatase nanopowder, < 25 nm particle size, 99.7% trace metals basis, Sigma-Aldrich) and PAT samples treated at 250 °C, 300 °C. It can be noted that even after 1 h at 300 °C, there are no peaks related to the anatase phase, appearing only some peaks related to the sample holder. On the other hand, when the microwave-assisted hydrothermal treatment was performed at 170 °C, the TiO_2 anatase phase was formed within the first minutes of reaction.

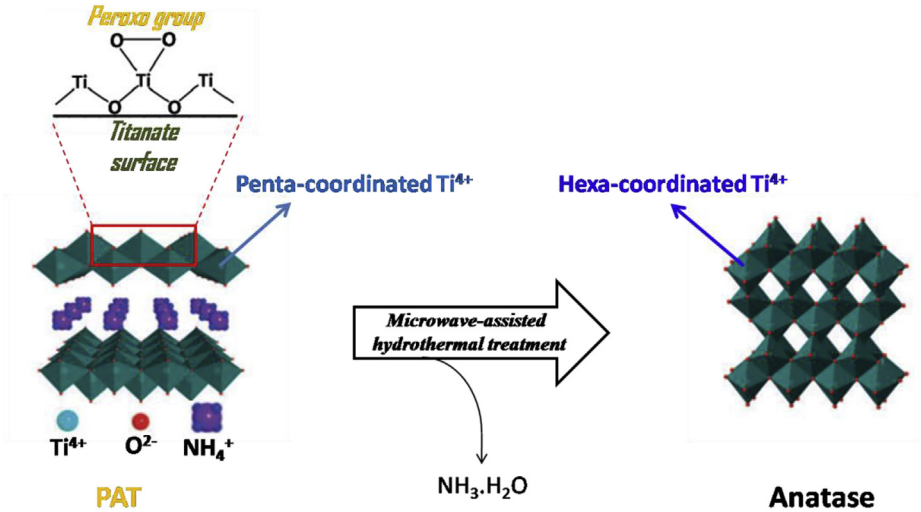

Scheme 1. Anatase formation from PAT under microwave-assisted hydrothermal treatment. The ammonium ions diffuse through the solution and further they are released from the solution as ammonia gas. Therefore, the system becomes poor in positively charged ammonium ions which are necessary to stabilize the negatively charged titanate layers, thereby resulting in anatase TiO_2 formation.

Additionally, the final sample powder acquired a white color, suggesting the full decomposition of the peroxogroups, as confirmed by previous analysis [48]. This is an indicative that a medium capable of releasing ammonium ion is required for anatase TiO_2 formation. The microwave-assisted hydrothermal method fulfills this requirement.

The second experiment consisted in the dispersion of PAT in benzyl alcohol (BnOH), which is not a solvent for NH_4^+ ions, with subsequent hydrothermal treatment using the same conditions applied for the anatase synthesis. XRD measurements performed on the obtained samples are shown in Fig. 8 (b). The results did not indicate the presence of the anatase TiO_2 in the samples. On the other hand, peaks related to titanate phase became more defined. These results confirm the hypothesis that the anatase phase formation occurs via release of ammonium ions and peroxogroups decomposition from the titanate-like structure.

The influence of the structural changes on the TiO_2 properties was examined with basis on the well-known TiO_2 photoactivity under UV-light. The main goal of this analysis was to confirm the crystallinity of the synthesized material formed, and not the obtainment of a high performance photocatalyst. This was attained using Rhodamine B dye (RhB) degradation as a probe system. Fig. 9 presents the results of RhB removal as a function of time with or without UV radiation exposure. The photoactivity of the samples containing surface peroxo groups has been reported in the literature [29,48]. However, this is not the unique

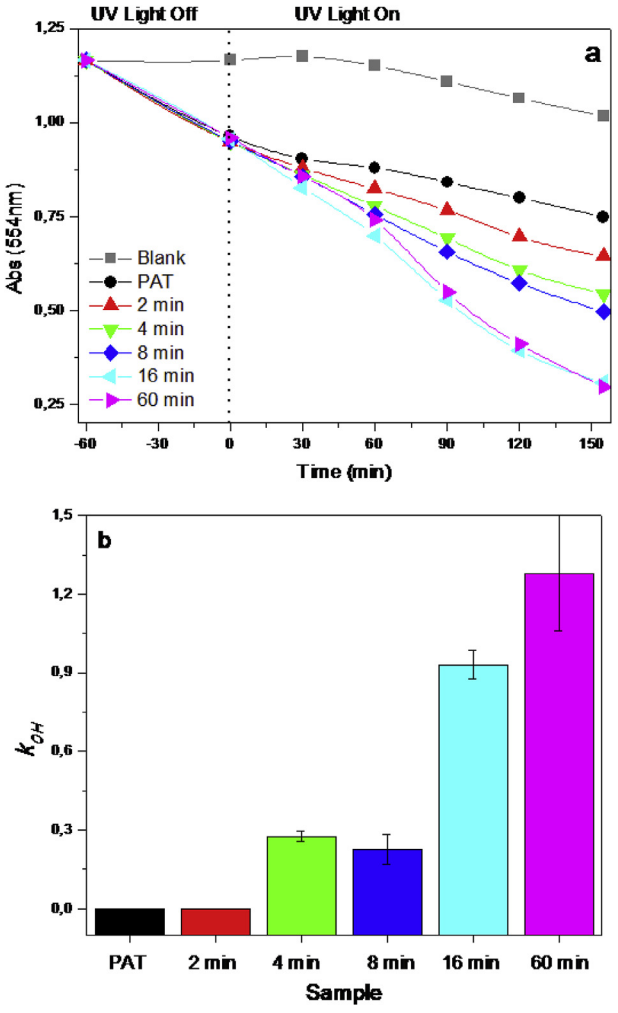

Fig. 9. a) Removal of RhB dye as a function of the time with and without UV radiation exposure. b) Formation of hydroxyl radicals (from 2-hydroxyterephthalic acid emission) by zero-order kinetics catalyzed by the as obtained samples.

requirement for photoactivity, as depicted by the results for PAT. As a matter of fact, the sample photoactivity increases with the increasing hydrothermal time, reaching a maximum for the sample treated at 16 min and remaining almost constant for longer times. Therefore, we can state that a reaction time for the synthesis using the proposed method as low as 16 min is enough to reach the maximum efficiency, as can be seen when comparing this sample with that one obtained after 60 min of reaction. This result agrees with the previous one, since these samples were only comprised of crystalline anatase TiO_2, without any detectable impurity. Also, it was observed that these samples correspond to nanoparticles with minor agglomeration.

One of the main photodegradation mechanisms is the attack of the organic dye molecule by hydroxyl radicals formed from the reaction between the ^-OH groups adsorbed onto the semiconductor surface and the positive hole in the semiconductor valence band, this latter being generated by photoexcitation [49]. Therefore, the ability of our samples to form hydroxyls radicals was checked by a method previously proposed to investigate the nanoparticle-catalyzed hydroxyl radical formation. This is represented by the k_{OH} values in Fig. 9(b), which is the slope of the 2-hydroxyterephthalic acid luminescence intensity vs. time plot [26,28]. As observed in Fig. 9(a), k_{OH} was proportional to the microwave-assisted hydrothermal treatment time due to the increasing content of anatase phase in the samples. Accordingly, we can suppose that the main mechanism in the photocatalytic RhB degradation is based mainly on the hydroxyl radical attack. Once all samples exhibited almost the same adsorption capability in the dark, the decreasing RhB light absorption at 554 nm is attributed to the dye photodegradation rather than adsorption.

The photodegradation mechanism based on hydroxyl radical ($^{\bullet}OH$) attack can be elucidated in terms of spontaneity by theoretical means. The anatase phase exhibits potential of 2.9 and −0.3 V *vs* NHE (Normal Hydrogen Electrode) for its valence band (VB) and conduction band (CB), respectively [50]. In this sense, it is possible to describe the reduction reaction as follows:

$$VB(h^+)_{TiO2} + e^- \rightarrow VB_{TiO2}\ E^\circ = 2.9\ V$$

$$^{\bullet}OH + e^- \rightarrow {}^-OH\ E^\circ = 1.6\ V$$

The first equation is related to the reduction of the positive hole in the TiO_2 VB, while the second equation relates to the reduction of the hydroxyl radical into hydroxyl anion. By combining both equations, one should obtain:

$$VB(h^+)_{TiO2} + {}^-OH \rightarrow VB_{TiO2} + {}^{\bullet}OH\ E^\circ = (2.9 - 1.6)\ V = 1.3\ V$$

Therefore, it is observed that the positive hole of the TiO_2 VB can generate hydroxyl radicals spontaneously (since $\Delta G = -nFE^\circ$), in agreement with the experimental data obtained in this work. Additionally, PAT contains surface peroxo groups, which could generate higher amounts of hydroxyl radicals, but these groups cannot be oxidized probably due to the PAT VB reduction potential.

Other TiO_2 polymorphs can be obtained by the pH adjustment in the synthesis, as proposed in this work [15,20]. Therefore, the obtaining of a TiO_2 mixed phase, or heterojunction, becomes feasible by adjusting a few synthesis parameters, as an attempt to create photocatalysts with better performances and different photodegradation mechanism [51].

4. Conclusions

The formation of anatase TiO_2 nanocrystals by OPM (Oxidant Peroxide Method) with subsequent microwave-assisted hydrothermal treatment has been described here. After a detailed characterization, it was confirmed that the PAT precursor exhibits a titanate-like structure comprised of NH_4^+ cations as counter ions for the anionic titanate layers, and surface peroxo groups. During the hydrothermal treatment, the NH_4^+ ions are released from PAT to the solution while anatase TiO_2 is formed concomitantly with the peroxogroup decomposition, due to a

rearrangement of the crystal structure. The surface PAT peroxo groups cannot prompt the hydroxyl radical formation, as shown by the photodegradation experiments. The photocatalytic performance of the samples was directly related to their anatase phase content. The results presented in this work highlight the mechanism involved in the anatase TiO_2 formation, which could be useful for the development of new synthesis approaches using the OPM-obtained titanium precursor with fine control on the crystal phase, morphology and facet crystal engineering.

Acknowledgements

The authors are grateful to the Ministry of Science, Technology, and Innovation (through SisNANO Program – National System of Laboratories in Nanotechnology), the National Council for Scientific and Technological Development (CNPq, Brazil China Virtual Center in Nanotechnology Project and grants #402287/2013-4, #468956/2014-0, #409904/2016-3, #407497/2018-8), Coordination for the Improvement of Higher Education Personnel (CAPES), Sao Paulo Research Foundation (FAPESP #18/01258-5, #15/14330-8, #16/09746-3), and Embrapa Rede AgroNano for their financial support. The authors also gratefully acknowledge the Laboratory for Multifunctional Materials/ETH-Zurich and the Head of Group Markus Niederberger for the laboratory facilities and Dr. Wei Cheng for the SEM measurements. The XANES spectra was measured at LNLS (project XAFS1-7797 and 9542), Campinas, SP, Brazil. The HRTEM measurements were performed at the Laboratorio de Microscopias Avanzadas (LMA) of the Instituto de Nanociencia de Aragon (INA) – Universidad de Zaragoza (Spain). W.A.Jr. also gratefully acknowledges the financial support provided by the Brazilian research funding agency CNPq (311463/2017-7). R.A. also gratefully acknowledges the support from the Spanish Ministerio de Economia y Competitividad (MAT2016-79776-P), from the Government of Aragon and the European Social Fund under the project “Construyendo Europa desde Aragon” 2014–2020 (grant number E/26). C.R. also acknowledges Chinese Academy of Sciences (CAS) President's International Fellowship Initiative (PIFI) by financial support and CAPES/Alexander von Humboldt Foundation by Experienced Research Fellowship (CAPES Finance Code 001; CAPES Process 88881.145566/2017-1).

References

[1] N.T.K. Thanh, N. Maclean, S. Mahiddine, Mechanisms of nucleation and growth of nanoparticles in solution, Chem. Rev. 114 (2014) 7610–7630.
[2] E.V. Savinkina, L.N. Obolenskaya, G.M. Kuzmicheva, I.D. Morozov, Effects of peroxo precursors and annealing temperature on properties and photocatalytic activity of nanoscale titania, J. Mater. Res. 33 (2018) 1422–1432.
[3] H.A.J.L. Mourão, O.F. Lopes, A.R. Malagutti, E.C. Paris, C. Ribeiro, Hydrothermal synthesis and photocatalytic properties of anatase TiO_2 nanocrystals obtained from peroxytitanium complex precursor, Mater. Sci. Semicond. Process. 25 (2014) 320–329.
[4] W. Avansi, R. Arenal, V.R. de Mendonça, C. Ribeiro, E. Longo, Vanadium-doped TiO_2 anatase nanostructures: the role of V in solid solution formation and its effect on the optical properties, CrystEngComm 16 (2014) 5021–5027.
[5] O.F. Lopes, K.T.G. Carvalho, G.K. Macedo, V.R. de Mendonça, W. Avansi, C. Ribeiro, Synthesis of $BiVO_4$ *via* oxidant peroxo-method: insights into the photocatalytic performance and degradation mechanism of pollutants, New J. Chem. 39 (2015) 6231–6237.
[6] X. Li, L. Xu, X. Li, M. Hu, R. Huang, C.J. Huang, Oxidant peroxo-synthesized monoclinic $BiVO_4$: insights into the crystal structure deformation and the thermochromic properties, Alloy. Comp. 787 (2019) 666–671.
[7] E.R. Camargo, M.G. Dancini, M.J. Kakihana, The oxidant peroxo method (OPM) as a new alternative for the synthesis of lead-based and bismuth-based oxides, J. Mater. Res. 29 (2014) 131–138.
[8] E.R. Camargo, M.J. Kakihana, Lead Hafnate ($PbHfO_3$) perovskite powders synthesized by the oxidant peroxo method, J. Am. Ceram. Soc. 85 (2002) 2170-2109.
[9] O.F. Lopes, E.C. Paris, C. Ribeiro, Synthesis of Nb_2O_5 nanoparticles through the oxidant peroxide method applied to organic pollutant photodegradation: a mechanistic study, Appl. Catal., B 144 (2014) 800–808.
[10] F. Idrees, R. Dillert, D. Bahnemann, F.K. Butt, M. Tahir, In-Situ synthesis of Nb_2O_5/g-C_3N_4 heterostructures as highly efficient photocatalysts for molecular H_2 evolution under solar illumination, Catalysts 9 (2019) 169–185.
[11] W. Avansi, V.R. de Mendonça, O. Lopes, C. Ribeiro, Vanadium pentoxide 1-D nanostructures applied to dye removal from aqueous systems by coupling adsorption and visible-light photodegradation, RSC Adv. 5 (2015) 12000–12006.
[12] I.A. Castro, W. Avansi, C. Ribeiro, WO_3/TiO_2 heterostructures tailored by the oriented attachment mechanism: insights from their photocatalytic properties, CrystEngComm 16 (2014) 1514–1524.
[13] W. Avansi, C. Ribeiro, E.R. Leite, V.R. Mastelaro, An efficient synthesis route of $Na_2V_6O_{16}{\cdot}nH_2O$ nanowires in hydrothermal conditions, Mater. Chem. Phys. 127 (2001) 56–61.
[14] A.E. Nogueira, E. Longo, E.R. Leite, E.R. Camargo, Synthesis and photocatalytic properties of bismuth titanate with different structures via oxidant peroxo method (OPM), J. Colloid Interface Sci. 415 (2014) 89–94.
[15] V.R. de Mendonça, C. Ribeiro, Influence of TiO2 morphological parameters in dye photodegradation: a comparative study in peroxo-based synthesis, Appl. Catal., B 105 (2011) 298–305.
[16] S.I. Seok, M. Vithal, J.A. Chang, Colloidal TiO_2 nanocrystals prepared from peroxotitanium complex solutions: phase evolution from different precursors, J. Colloid Interface Sci. 346 (2010) 66–71.
[17] M. Nag, S. Ghosh, R.K. Rana, S.V. Manorama, Controlling phase, crystallinity, and morphology of titania nanoparticles with peroxotitanium complex: experimental and theoretical insights, J. Phys. Chem. Lett. 1 (2010) 2881–2885.
[18] E.R. Camargo, M. Kakihana, Peroxide-Based route free from halides for the synthesis of lead titanate powder, Chem. Mater. 13 (2001) 1181–1184.
[19] P. Tengvall, T.P. Vikinge, I. Lundström, B. Liedberg, FT-Raman spectroscopic studies of the degradation of titanium peroxy gels made from metallic titanium and hydrogen peroxide, J. Colloid Interface Sci. 160 (1993) 10–15.
[20] C. Ribeiro, C.M. Barrado, E.R. Camargo, E. Longo, E.R. Leite, Phase transformation in titania nanocrystals by the oriented attachment mechanism: the role of the pH value, Chem. Eur J. 15 (2009) 2217–2222.
[21] G. Schwarzenbach, J. Muehlebach, K. Mueller, Peroxo complexes of titanium, Inorg. Chem. 9 (1970) 2381–2390.
[22] Y. Wang, A.S. Ganeshraja, C. Jin, K. Zhu, J. Wang, One-pot synthesis visible-light-active TiO2 photocatalysts at low temperature by peroxotitanium complex, J. Alloy. Comp. 765 (2018) 551–559.
[23] I. Bilecka, M. Niederberger, Microwave chemistry for inorganic nanomaterials synthesis, Nanoscale 2 (2010) 1358–1374.
[24] S.G. Kumar, K.R.S.A. Rao, Polymorphic phase transition among the titania crystal structures using a solution-based approach: from precursor chemistry to nucleation process, Nanoscale 6 (2014) 11574–11632.
[25] H.A.J.L. Mourão, W. Avansi, J.E. Oliveira, E.S. Fimiano, C. Ribeiro, A study of the precursors and photoactivity of nanostructures of Ti oxides synthesized by the alkaline hydrothermal method, Sci. Adv. Mater. 5 (2013) 71–85.
[26] V.R. de Mendonça, H.A.J.L. Mourão, A.R. Malagutti, C. Ribeiro, The role of the relative dye/photocatalyst concentration in TiO_2 assisted photodegradation process, Photochem. Photobiol. 90 (2014) 66–72.
[27] K. Ishibashi, A. Fujishima, T. Watanabe, K. Hashimoto, Detection of active oxidative species in TiO_2 photocatalysis using the fluorescence technique, Electrochem. Commun. 2 (2002) 207–210.
[28] V.R. de Mendonça, C.J. Dalmaschio, E.R. Leite, M. Niederberger, C. Ribeiro, Heterostructure formation from hydrothermal annealing of preformed nanocrystals, J. Mater. Chem. 3 (2015) 2216–2225.
[29] P. Francatto, F.N. Souza Neto, A.E. Nogueira, A.M. Kubo, L.S. Ribeiro, L.P. Gonçalves, L.F. Gorup, E.R. Leite, E.R. Camargo, Enhanced reactivity of peroxo-modified surface of titanium dioxide nanoparticles used to synthesize ultrafine bismuth titanate powders at lower temperatures, Ceram. Int. 42 (2016) 15767–15772.
[30] T. Kasuga, M. Hiramatsu, A. Hoson, T. Sekino, K. Niihara, Titanium Oxide nanorods pH sensors: comparison between voltammetry and extended gate field effect transistor measurements, Lagmuir 14 (1998) 3160–3163.
[31] J. Zhang, M.J. Li, Z.C. Feng, J. Chen, C.J. Li, UV Raman Spectroscopic Study on TiO_2. I. Phase transformation at the surface and in the bulk, Phys. Chem. B. 110 (2006) 927–935.
[32] J. Xie, X. Wang, Y.J. Zhou, Understanding formation mechanism of titanate nanowires through hydrothermal treatment of various Ti-containing precursors in basic solutions, Mater. Sci. Technol. 28 (2012) 488–494.
[33] R.A. Zárate, S. Fuentes, J.P. Wiff, V.M. Fuenzalida, A.L. Cabrera, Chemical composition and phase identification of sodium titanate nanostructures grown from titania by hydrothermal processing, J. Phys. Chem. Solids 68 (2007) 628–637.
[34] N. Zhang, G. Li, S. Wang, X. Xu, L. Li, TaCxOy: a photocatalytic promoter on g-C3N4 for visible-light Cr6+ reduction, Catal. Commun. 119 (2019) 129–133.
[35] V.R. de Mendonça, O.F. Lopes, R. Fregonesi, T. Giraldi, C. Ribeiro, TiO_2-SnO_2 heterostructures applied to dye photodegradation: the relationship between variables of synthesis and photocatalytic performance, Appl. Surf. Sci. 298 (2014) 182–191.
[36] M.K. Chaudhuri, B. Das, Direct synthesis of alkali-metal and ammonium pentafluoroperoxytitanates(IV), $A_3[Ti(O_2)F_5]$, and first synthesis and structural assessment of alkali-metal and ammonium difluorodiperoxytitanates (IV), $A_2[Ti(O_2)_2F_2]$, Inorg. Chem. 25 (1986) 168–170.
[37] J.P. Mathieu, H. Poulet, Les frequences fondamentales de vibration de l'ion NH_4^+, Spectrochim. Acta 16 (1960) 696–703.
[38] T.L. Hanley, V. Luca, I. Pickering, R.F. Howe, Structure of titania sol − gel films: a study by X-ray absorption spectroscopy, J. Phys. Chem. B 106 (2002) 1153–1160.
[39] L.X. Chen, T. Rajh, Z. Wang, M.C. Thurnauer, XAFS Studies of surface structures of TiO_2 nanoparticles and photocatalytic reduction of metal ions, J. Phys. Chem. B 101 (1997) 10688–10697.
[40] C. Ribeiro, C. Villa, D.B. Stroppa, V.R. Mastelaro, J. Bettini, E. Longo, E. Leite, Anisotropic growth of oxide nanocrystals: insights into the rutile TiO_2 phase, J.

Phys. Chem. C 111 (2007) 5871–5875.
[41] F. Farges, G.E. Brown, J. Rehr, Ti K-edge XANES studies of Ti coordination and disorder in oxide compounds: comparison between theory and experiment, J. Phys. Rev. B. 56 (1997) 1809–1819.
[42] B. Zhao, L. Lina, D. He, Phase and morphological transitions of titania/titanate nanostructures from an acid to an alkali hydrothermal environment, J. Mater. Chem. A. 1 (2013) 1659–1668.
[43] A. Song, D. Jing, M.A. Hines, Rutile surface reactivity provides insight into the structure-directing role of peroxide in TiO_2 polymorph control, J. Phys. Chem. C 118 (2014) 27343–27352.
[44] B. Zhao, F. Chen, X. Gu, J. Zhang, Organic-Stabilizer-Free synthesis of layered protonic titanate nanosheets, Chem. Asian J. 5 (2010) 1546–1549.
[45] N. Sutradhar, A. Sinhamahapatra, S.K. Pahari, H.C. Bajaj, A.B. Panda, Room temperature synthesis of protonated layered titanate sheets using peroxo titanium carbonate complex solution, Chem. Commun. 47 (2011) 7731–7733.
[46] T. Kasuga, M. Hiramatsu, A. Hoson, T. Sekino, K. Niihara, formation of titanium oxide nanotube, Langmuir 14 (1998) 3160–3163.
[47] a) B. Zhao, F. Chen, Y. Jiao, J. Zhang, Phase transition and morphological evolution of titania/titanate nanomaterials under alkalescent hydrothermal treatment, J. Mater. Chem. 20 (2010) 7990–7997;
b) Y. Jiao, B. Zhao, F. Chen, J. Zhang, Insight into the crystal lattice formation of brookite in aqueous ammonia media: the electrolyte effect, CrystEngComm 13 (2011) 4167–4173.
[48] A.E. Nogueira, L.S. Ribeiro, L.F. Gorup, G.T.S.T. Silva, F.F.B. Silva, C. Ribeiro, E.R. Camargo, New approach of the oxidant peroxo method (opm) route to obtain ti $(oh)_4$ nanoparticles with high photocatalytic activity under visible radiation, Int. J. Photoenergy 2018 (2018) 1–10.
[49] H.A.J.L. Mourão, V.R. de Mendonça, A.R. Malagutti, C. Ribeiro, Nanostructures in photocatalysis: a review about synthesis strategies of photocatalysts in nanometric size, Quím. Nova 32 (2009) 2181–2190.
[50] Y. Xu, M.A.A. Schoonen, The absolute energy positions of conduction and valence bands of selected semiconducting minerals, Am. Mineral. 85 (2000) 3–4.
[51] S. Wang, H. Yu, S. Yuan, Y. Zhao, Z. Wang, J. Fang, M. Zhang, L. Shi, Synthesis of triphasic, biphasic, and monophasic TiO_2 nanocrystals and their photocatalytic degradation mechanisms, Res. Chem. Intermed. 42 (2016) 3775–3788.